A&A 556, A79 (2013)
DOI: 10.1051/0004-6361/201321787

Astronomy & Astrophysics

Hot coronal loops associated with umbral brightenings⋆

C. E. Alissandrakis and S. Patsourakos

Department of Physics, University of Ioannina, 45110 Ioannina, Greece
e-mail: [calissan;spatsour]@cc.uoi.gr

Received 26 April 2013 / Accepted 21 June 2013

ABSTRACT

Aims. We aim to investigate the association of umbral brightenings with coronal structures.
Methods. We analyzed AIA/SDO high-cadence images in all bands, HMI/SDO data, soft X-ray images from SXI/GOES-15, and Hα images from the GONG network.
Results. We detected umbral brightenings that were visible in all AIA bands as well as in Hα. Moreover, we identified hot coronal loops that connected the brightenings with nearby regions of opposite magnetic polarity. These loops were initially visible in the 94 Å band, subsequently in the 335 Å band, and in one case in the 211 Å band. A differential emission measure analysis revealed plasma with an average temperature of about 6.5×10^6 K. This behavior suggests cooling of impulsively heated loops.

Key words. sunspots – Sun: corona – Sun: magnetic topology

1. Introduction

Sunspots are the site of many dynamic phenomena, such as umbral oscillations, running umbral/penumbral waves, and umbral flashes (see review by Solanki 2003). Beckers & Tallant (1969) used the term *umbral flashes* to describe small (average diameter of 2200 km), short-lived (<120 s) bright structures that they observed in the K line. They noticed a tendency of these flashes to repeat every 145 s, which led many subsequent authors to identify them with the *umbral oscillations* discovered later by Bhatnagar & Tanaka (1972), Beckers & Schultz (1972) and Giovanelli (1972); however, the time profiles of umbral flashes presented by Beckers & Tallant (1969) did not have a sinusoidal form, but showed a fast rise followed by a slower decay with a characteristic time of ∼50 s.

Umbral flashes are difficult to observe in other chromospheric lines in the visible part of the spectrum. One case in Hα was reported by Alissandrakis et al. (1992). These authors were also the first to report on waves propagating from inside the umbra outward to become penumbral waves (Zirin & Stein 1972; Giovanelli 1972). The propagating nature of umbral waves was subsequently verified by Alissandrakis et al. (1998) and Tsiropoula et al. (2000).

Another type of umbral brightenings, termed *umbral flares*, was reported by Tang (1978). They appear in Hα as bright patches confined inside the umbra, with the other footpoint located in the nearby plage; they last for 25−45 min and are sometimes accompanied by type III bursts.

An important aspect of sunspot-associated dynamic phenomena is their extension in the upper layers of the solar atmosphere. Indeed, Gelfreikh et al. (1999) detected sunspot oscillations at 1.7 cm with the Nobeyama radioheliograph, while Nindos et al. (2002) resolved them spatially using the VLA. The availability of continuous high-cadence, high-resolution observations of the entire sun from instruments onboard the Solar Dynamics Observatory (SDO) gives an excellent opportunity for detailed studies of sunspot-associated phenomena in the transition region and the corona (e.g. Reznikova et al. 2012).

In this article we used AIA/SDO data to investigate the extension of umbral brightenings into the transition region and the low corona. We describe the observations in Sect. 2 and discuss the results in Sect. 3.

2. Observations and results

We examined SDO/AIA images of a number of isolated, well-developed symmetric sunspots with the help of the *Helioviewer* site for the occurrence of brightenings above their umbra. We found several cases, best visible in the 1600 Å band, and selected two for more detailed study (Table 1); for this study we used cutouts of the original high-cadence images.

2.1. Event of January 19, 2013

A well-observed case is the event of January 19, 2013. Figure 1 shows a set of images in selected AIA wavelength bands together with HMI images of continuum intensity, longitudinal magnetic field, and line-of-sight velocity, as well as an Hα image from the GONG network, during the peak of the brightening. The bottom row shows images from which the intensity before the event was subtracted for better visibility of the brightening.

The brightening, located 3″ N of the spot center, is visible in all AIA bands; it is barely visible in the lower-resolution Hα difference image and there is no trace of it in the continuum, B_ℓ and v_ℓ images, not even in the image of the line depth of the FeI 6173 Å line used by HMI (not shown here). Thus the lower extent of the brightening is somewhere between the formation height of the core of the FeI line (∼302 km, see Norton et al. 2006) and of the 1700 Å band (∼360 km, see Fossum & Carlsson 2005). We found no indication of associated type III burst activity in the CALLISTO and WIND/WAVES data bases. The peak intensity of the brightening relative to the one before the event

⋆ Two movies are available in electronic from at http://www.aanda.org

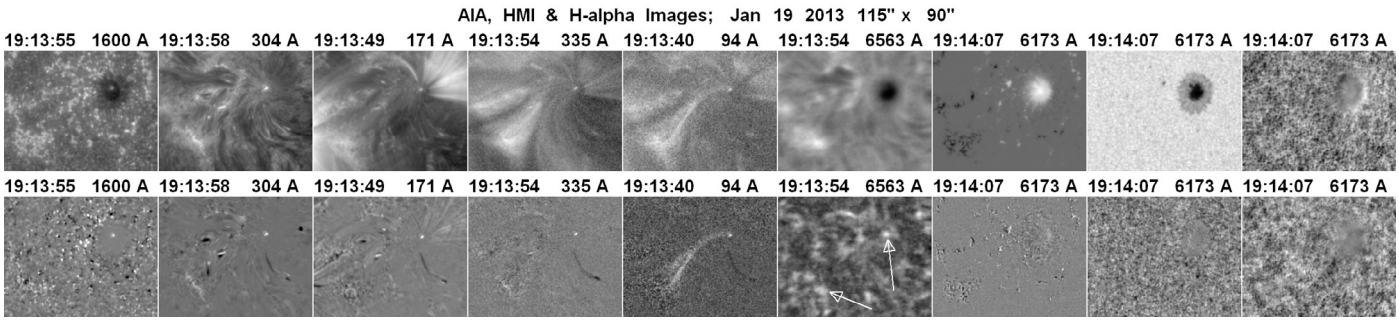

Fig. 1. Umbral brightening of January 19, 2013 in selected AIA bands and Hα, together with HMI images of the longitudinal magnetic field, continuum intensity, and line-of-sight velocity. The *bottom row* shows difference images. The arrows in the Hα difference image point to the umbral brightening and the associated plage footpoint. The images are orientated in the solar E-W/N-S direction. A time sequence of images is shown in movie 1 in the electronic version of the journal. Each frame of the movie shows images in the 1600 and 304 Å bands (*top row*) as well as in the 94 and 335 Å AIA bands (*bottom row*); the first frame shows direct images in all four bands, the others show difference images in all bands except 1600 Å.

Table 1. List of observations.

Date	Region	Location	Peak UT
2013 Jan. 19	1658	W15.7 S12.0	19:14
2012 Sep. 30	1579	E01.8 S10.0	07:53

Table 2. Peak intensity of brightenings relative to the local background.

Band	2013 Jan. 19	2012 Sep. 30, E	2012 Sep. 30, W
1700	1.86	–	1.53
1600	4.70	1.73	3.25
304	3.74	3.00	3.08
171	3.12	1.25	2.94
211	2.66	1.90	1.48
193	2.53	1.62	2.30
131	3.26	2.50	3.08
335	2.81	1.78	2.25
94	3.00	2.26	1.80

is given in Table 2; the brightening is strongest in the 1600 Å band where its intensity is higher than that of the quiet Sun and similar to the average intensity of plage regions; the brightening is weakest in the 1700 Å band.

At the time of its peak, the brightening had a rather simple structure (Fig. 2), with small differences among the AIA spectral bands. It was roughly elliptical in shape, with a FWHM of 2.4″ by 1.4″ in the 171 Å image, with an arch-like extension NE; the structure was more compact in the 304, 335, and 94 Å images, with the peak displaced slightly to the NW and some indication of a second peak.

The most interesting aspect of the brightening is that in the 94 Å band image, with a characteristic temperature of $\log T \sim 6.8$ (Lemen et al. 2012), it is clearly associated with a coronal loop (Fig. 1), best seen in the subtracted image. The loop ends in a region of opposite polarity at a projected distance of 53″, which is bright in Hα, and in the 304 Å and some other AIA bands. This opposite footprint is more extended than the brightening, and the cross-section of the loop along its length varies accordingly. This is consistent with the expected variation of the magnetic field strength from the sunspot to the plage.

The loop developed together with the brightening and was not detected in any other spectral band up to the maximum of the brightening. After that, the loop became progressively visible in

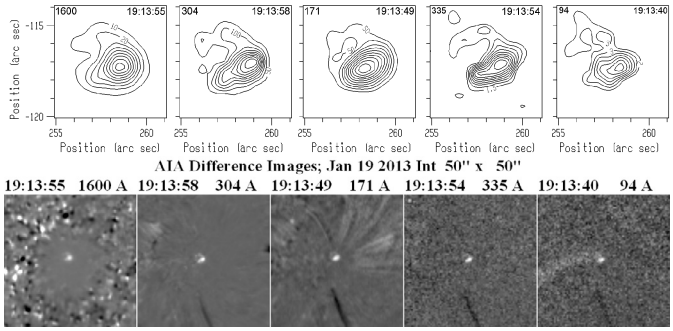

Fig. 2. Contour plots and difference images of the brightening at the time of its maximum.

the 335 Å band (characteristic temperature of $\log T \sim 6.4$), while it faded away in the 94 Å band (Fig. 3). Note that the loop persisted for several minutes after the brightening had faded away. Also note that the overall geometry of the loop and its footpoints is very well depicted in the images of the rms variation of the intensity (last row in Fig. 3).

No observations from Hinode were available at the time of the event. Soft X-ray images from SXI on GOES-15 show the loop in all channels, starting around 09:10 UT with a peak near the peak of the umbral brightening.

Figure 4 shows the time profiles of the brightening of two portions of the loop and of its southern footpoint. The time profiles of the brightening and the S footpoint during the decay phase in 94 and 335 Å are probably contaminated by the loop emission. The brightening had two main peaks, a fast rise of a few minutes and a much longer decay. The duration of the main phase was shortest in the 1600 Å band (~10 min). The S footpoint appeared almost simultaneously with the brightening at 304 Å, with a delay of ~1 min in the rising phase and ~3 min in the peak.

In the 94 Å band the S and the N portions of the loop showed practically identical light curves, both delayed by ~6 min with respect to the peak of the brightening. In 335 Å the S footpoint appeared first, ~12 min after the peak of the brightening, followed by the S part of the loop after ~3 min and the N part of the loop ~7 min later. Compared with the 94 Å band, the N part of the loop in 335 Å was delayed by ~18 min and the S part by ~12 min.

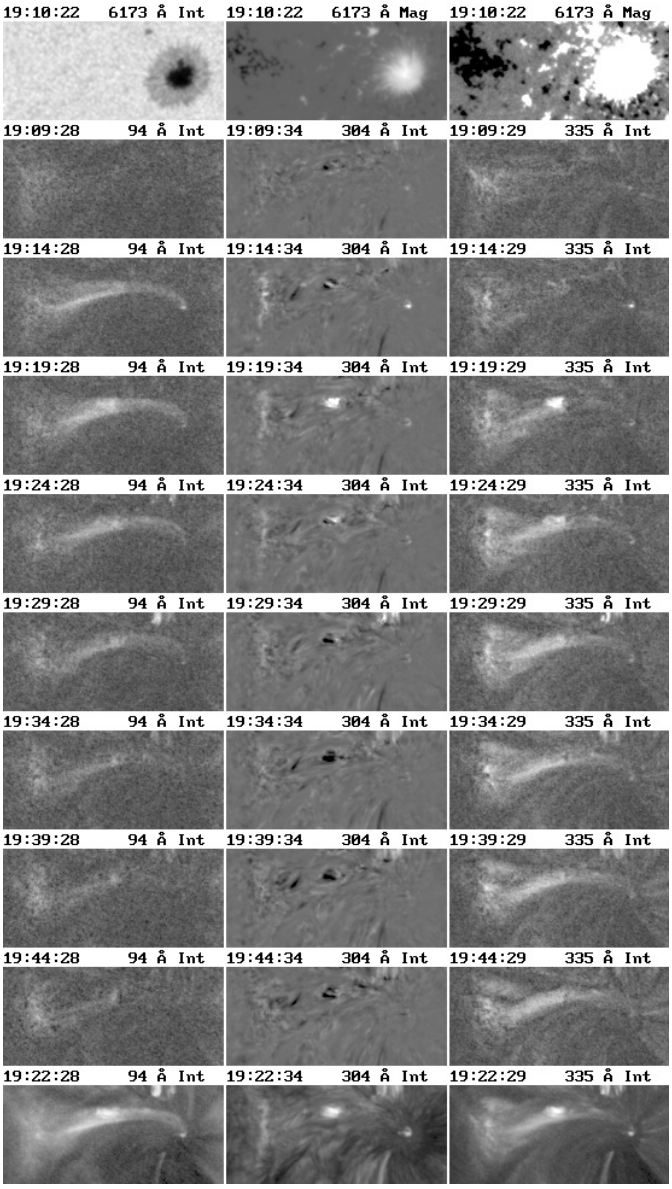

Fig. 3. Time sequence of difference images in the AIA 94, 304, and 335 Å bands over a field of view of 100″ by 45″. The last row shows images of the intensity rms during the sequence (19:00 to 19:45 UT), while the first row shows HMI images of continuum intensity and longitudinal magnetic field, saturated at ±100 G in the right column. The 335 and 94 Å images are one minute averages to reduce noise. The small bright structure near the middle of the loop is an unrelated phenomenon. The images have been rotated by 39° with respect to the solar E-W direction.

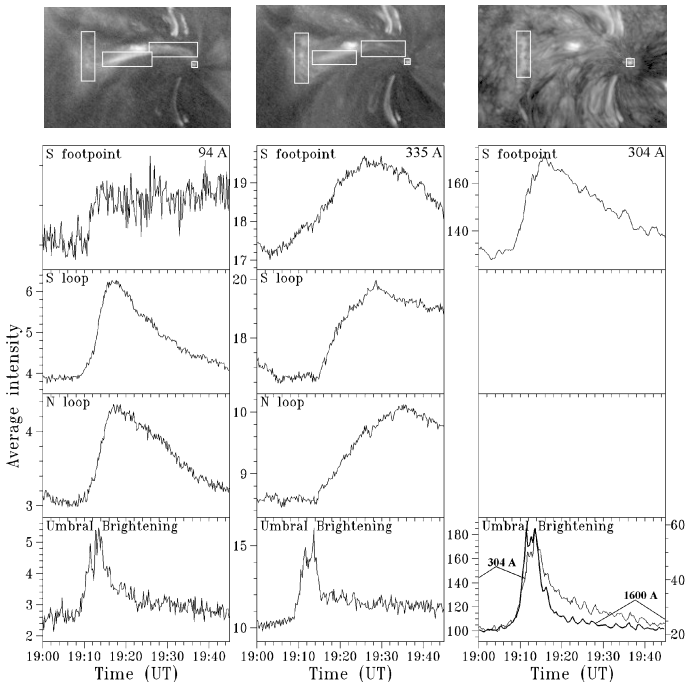

Fig. 4. Time profiles of the brightening, the southern footpoint and two portions of the loop. The boxes in the *top row* images show the corresponding regions in rms images (from *left to right*: S footpoint, S loop, N loop, umbral brightening).

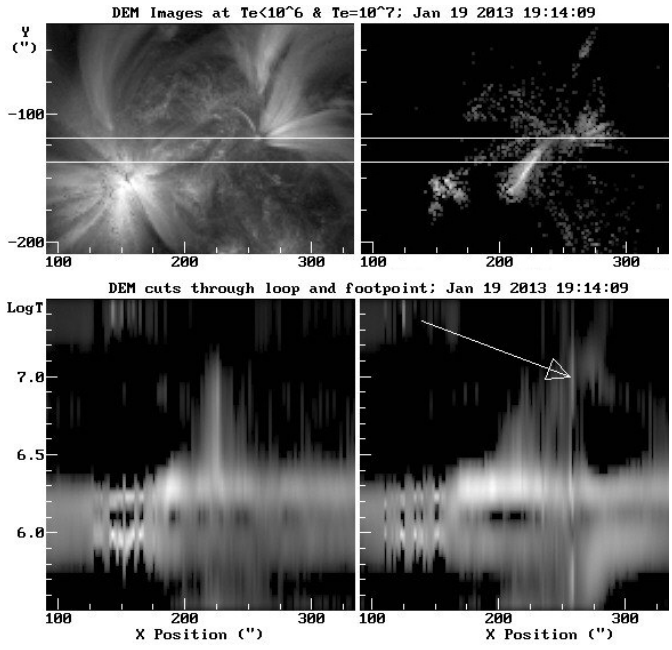

Fig. 5. Differential emission measure maps for $T < 10^6$ K and $T = 10^7$ K (*top*). The *bottom row* shows the DEM as a function of position and temperature along the lines marked in the images at the top. The arrow marks the position of the brightening.

To quantify the temperature structure of the loop we performed a differential emission measure (DEM) analysis based on the coronal AIA channels, using the method described in Plowman et al. (2013). Our results are presented in Fig. 5, which shows DEM images of the region for temperatures below 10^6 K and at 10^7 K; in the first image the loop is invisible, while in the other it stands out clearly above the surrounding plasma. In the DEM images as a function of position and temperature shown in the bottom row of the figure, the bulk of the background plasma is in the temperature range $5.75 < \log T < 6.4$. In the lower left panel, where the DEM is displayed along a line crossing the loop at its middle, the loop appears at $x \sim 225$ as an excursion of the DEM to high temperatures; the DEM peaks at $\log T \sim 6.82$ ($T \sim 6.5 \times 10^6$ K). The lower right panel of Fig. 5 shows the DEM along a line crossing the umbral brightening at $x = 258$; here the DEM also extends to high temperatures, with a maximum at $\log T \sim 6.96$.

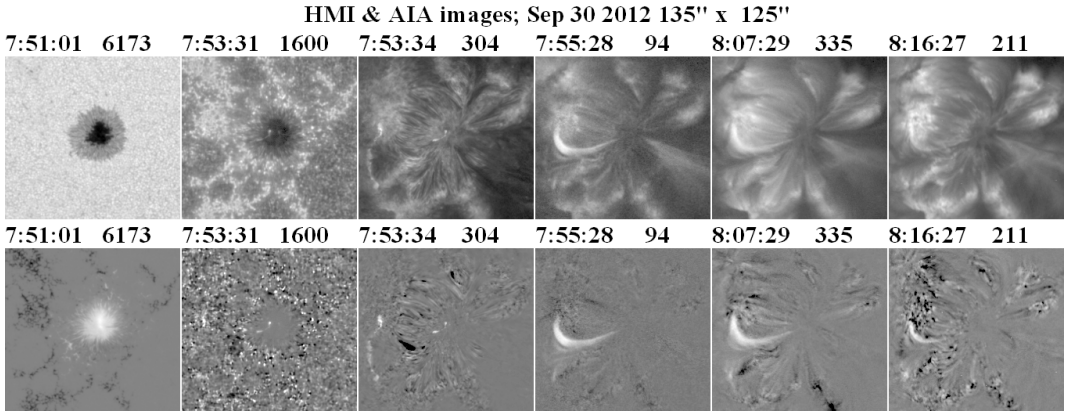

Fig. 6. Umbral brightening of September 30, 2012 in selected AIA bands. 1600 and 304 Å images are at the peak of the brightening, 94, 335, and 211 Å images are at the peak of the associated coronal loop. 94 and 335 Å images are 1-min averages to reduce noise. The *bottom row* shows difference images. The *first column* shows HMI images of continuum intensity and longitudinal magnetic field. The time evolution of this loop and its footpoins is shown in movie 2 of the electronic version of the journal. Each frame of the movie shows difference images in the 1600 and 304 Å bands (*top row*) as well as in the 94 and 335 Å AIA bands (*bottom row*).

2.2. Event of September 30, 2012

A similar event was observed on September 30, 2012 in active region 1759 (Fig. 6). This brightening consisted of two patches, 10″ apart, connected by a faint emission bridge that gave them a sickle-like appearance. The E patch started near the umbra-penumbra boundary and extended to the middle of the penumbra, the W patch was entirely within the umbra, ∼5″ away from its center; their sizes were roughly 4 by 1.5″ and 5 by 2″ respectively, but both contained up to four smaller components, down to 1″ size. A very weak type III burst was discernible during the rise phase of the W patch, at 07:51:09 UT in the San Vito dynamic spectra below 60 MHz and in the WIND/WAVES RAD2 spectra (07:51 UT at 13.8 MHz and 07:52 UT at 2 MHz); lacking imaging data, we cannot associate them with certainty with the event.

The coronal loop started near the umbra-penumbra boundary, at the west end of the E patch and extended over 44″ to the adjoining opposite polarity plage. The plage footpoint was visible not only in the 304 Å band, but also in the 1600 Å band (Fig. 6); it was also visible in the GONG difference Hα image, where the brightening itself was not. The time evolution of this loop is similar to that of the event of January 19, 2013: it was best visible in the 94 Å band, ∼2 min after the maximum of the umbral brightening and in the 335 Å band ∼12 min later. Here we also had emission in the 211 Å band (characteristic temperature of $\log T \sim 6.3$), which peaked ∼23 min after the brightening. Soft X-ray images from GOES SXI showed a picture similar to that of the January 19 2013 event: the hot loop was visible in all SXI channels and appeared at about the same time as the 94 Å loop.

The light curve of the brightening itself had a fluctuating character, with the bulk of the emission lasting for ∼8 min in the 1600 Å band. The peak intensities of the E and W components of the brightening relative to the local background are given in Table 2.

The results of our DEM analysis are shown in Fig. 7 at three instances during the evolution of the event. The background plasma now is near $\log T \sim 6.3$ and the cuts shown in the bottom row of the Figure cross the loop at two points, at $x = -80$ and $x = -45$; the DEM on the loop has a maximum at $\log T \sim 6.86$. Note also the gradual cooling of the loop between 07:53 UT and 08:15 UT.

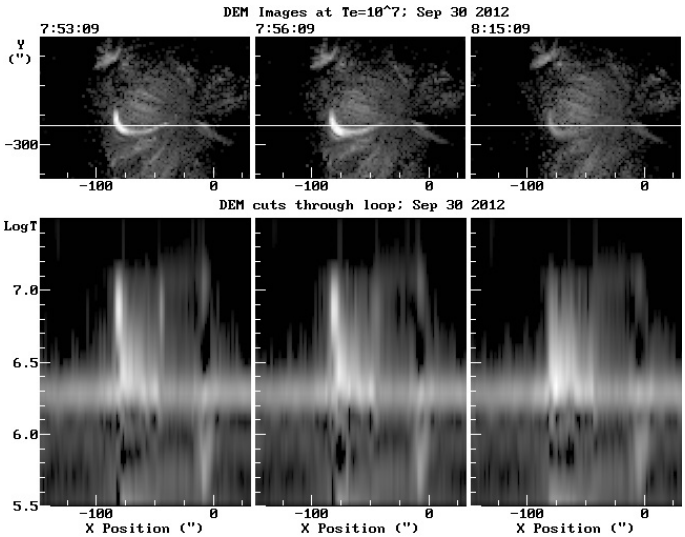

Fig. 7. Differential emission measure maps for $T = 10^7$ K at three instances during the event of September 30, 2012 (*top*). The *bottom row* shows the DEM as a function of position and temperature along the line marked in the images at the top.

3. Summary and discussion

Our analysis of short-lived umbral brightenings from SDO/AIA data showed two cases where the brightenings were not confined to the low atmospheric layers. Not only were they visible in all AIA channels, which implies a very extended temperature range, but they were also connected by hot coronal loops to opposite-polarity footpoints located ∼50″ away. The association of these brightenings with hot coronal loops proves beyond any doubt that their origin is magnetic. In this respect, they are similar to the umbral flares reported by Tang (1978), but they are more compact and of shorter duration. The brightenings were strongest in the 1600 Å AIA band, where their intensity exceeded that of the quiet Sun and reached the average level of the plage. They did not appear in the HMI images, and we estimate their lowest extent to a height between 302 km and 360 km.

We note briefly that the association with hot coronal loops is not a general property of umbral brightenings. We have found several cases that did not exhibit such an association (see, e.g. the

bright point at $x = -26, y = -274$ at 07:42 UT in movie 2); these were shorter (∼1 min) and probably similar to the umbral flashes of Beckers & Tallant (1969). We are currently preparing a report on them.

The associated hot coronal loops appeared first in the 94 Å AIA band, where they reached maximum 2 to 6 min after the brightening maximum. Subsequently, they became visible in the 335 Å band and, in the case of the September 30 2012 event, in the 211 Å band. In the GOES-15 SXI soft X-ray images the loop was visible in all bands with a peak near that of the 94 Å loop. This behavior is suggestive of gradual cooling of hot plasma.

The high temperature of the loops is confirmed not only by their appearance in the hot 94 Å channel and in the SXI images, but also by our DEM analysis, which showed that the average temperature of the loop plasma was $\sim 6.5 \times 10^6$ K. Thus the events presented here are clear examples of plasma cooling from high temperatures of several MK to ≈2.5 MK. The fact that the hot loops are rooted in sunspot umbrae is a key advantage of our data, since this allows direct observation of their footpoints without obscuration from low-lying structures. Obscuration is a limiting factor in observations of loops rooted in plages, where it is often hard to obtain a view of their footpoints and is difficult even to identify them. This is the case for several studies of hot evolving coronal loops in active regions using Hinode and AIA (e.g. Warren et al. 2011).

Cooling of individual coronal loops or even of large 2D fields in ARs has been observed in the past (e.g. Warren et al. 2003; López Fuentes et al. 2007; Ugarte-Urra et al. 2009; Viall & Klimchuk 2011; Warren et al. 2011). There are two possibilities to explain the cooling. One is that we may have a quasi-steady hot coronal loop that begins to cool down once its (quasi-steady) heating is shut off. This possibility can be safely excluded, because quasi-steady multi-million degrees hot coronal loops are expected to have intense footpoint emissions (e.g. Patsourakos & Klimchuk 2008). However, our observations of the umbral loop footpoints show that they are only a factor ≈2−3 more intense than the associated coronal sections. A second, more plausible scenario for the observed evolution is that the coronal-loop cooling follows its impulsive heating to multi-million K. It is possible that the heating phase cannot be observed due to the low emission measure associated with it: the temperature increase is not initially tracked by the loop density, because it takes some time to fill a coronal loop with hot plasma via chromospheric evaporated material (e.g. Patsourakos & Klimchuk 2006).

We point out here that high-frequency impulsive heating, with a repeat time between successive heating pulses shorter than the coronal cooling time, also leads to quasi-steady conditions. If this had been the case, one would expect re-heating of the observed loops. However, inspection of AIA movies spanning over 90 min after the appearance of the observed loops did not show strong evidence for this. The fact that the observed loops did not appear to cool down to the 211 channel and below may imply that they did not have enough emission to stand above the strong, highly-structured and dynamic active-region background observed in warmer emissions (≤2 MK). Our inferences above would be more firmly confirmed or rejected through detailed modeling of the observed loops, which is an important task for the future.

The relatively simple geometry of the hot loops and their footpoints as well as the possibility of following their temperature-density evolution through computating the DEM from AIA data makes these structures ideal for studying the heating and cooling of loops; we intend to do this in a future work.

Acknowledgements. The authors made extensive use of the data bases of SDO (AIA and HMI), GONG, GOES, CALLISTO, WIND/WAVES, the USAF RSTN network and the *Helioviewer* site (http://helioviewer.org); they are grateful to all those that worked for the development and operation of these instruments and for making the data available. The research of SP has been supported in part by the European Union (European Social Fund ESF) and in part by the Greek Operational Program "Education and Lifelong Learning" of the National Strategic Reference Framework (NSRF) – Research Funding Program: Thales "Hellenic National Network for Space Weather Research"-MIS 377274. S.P. also acknowledges support from an FP7 Marie Curie Grant (FP7-PEOPLE-2010-RG/268288).

References

Alissandrakis, C. E., Georgakilas, A. A., & Dialetis, D. 1992, Sol. Phys., 138, 93
Alissandrakis, C. E., Tsiropoula, G., & Mein, P. 1998, ASP Conf. Ser., 155, 49
Beckers, J. M., & Schultz, R. B. 1972, Sol. Phys., 27, 61
Beckers, J. M., & Tallant, P. E. 1969, Sol. Phys., 7, 351
Bhatnagar, A., & Tanaka, K. 1972, Sol. Phys., 24, 87
Fossum, A., & Carlsson, M. 2005, ApJ, 625, 556
Gelfreikh, G. B., Grechnev, V., Kosugi, T., & Shibasaki, K. 1999, Sol. Phys., 185, 177
Giovanelli, R. G. 1972, Sol. Phys., 27, 71
Lemen, J. R., Title, A. M., Akin, D. J., et al. 2012, Sol. Phys., 275, 17
López Fuentes, M. C., Klimchuk, J. A., & Mandrini, C. H. 2007, ApJ, 657, 1127
Nindos, A., Alissandrakis, C. E., Gelfreikh, G. B., Bogod, V. M., & Gontikakis, C. 2002, A&A, 386, 658
Norton, A. A., Graham, J. P., Ulrich, R. K., et al. 2006, Sol. Phys., 239, 69
Patsourakos, S., & Klimchuk, J. A. 2006, ApJ, 647, 1452
Patsourakos, S., & Klimchuk, J. A. 2008, ApJ, 689, 1406
Plowman, J., Kankelborg, C., & Martens, P. 2013, ApJ, 771, 2
Reznikova, V. E., Shibasaki, K., Sych, R. A., & Nakariakov, V. M. 2012, ApJ, 746, 119
Solanki, S. K. 2003, A&ARv, 11, 153
Tang, F. 1978, Sol. Phys., 60, 119
Tsiropoula, G., Alissandrakis, C. E., & Mein, P. 2000, A&A, 355, 375
Ugarte-Urra, I., Warren, H. P., & Brooks, D. H. 2009, ApJ, 695, 642
Viall, N. M., & Klimchuk, J. A. 2011, ApJ, 738, 24
Warren, H. P., Winebarger, A. R., & Mariska, J. T. 2003, ApJ, 593, 1174
Warren, H. P., Brooks, D. H., & Winebarger, A. R. 2011, ApJ, 734, 90
Zirin, H., & Stein, A. 1972, ApJ, 178, L85